Analytical Sciences (2022) 38:1105–1114
https://doi.org/10.1007/s44211-022-00140-4

ORIGINAL PAPER

Sensitivity enhancement in inductively coupled plasma mass spectrometry using nebulization methods via nitrogen mixed gas effect

Kayo Yanagisawa[1,2] · Makoto Matsueda[1,2] · Makoto Furukawa[1,3] · Yoshitaka Takagai[1,4]

Received: 31 March 2022 / Accepted: 24 May 2022 / Published online: 17 June 2022

Abstract
We demonstrate the sensitivity enhancement in inductively coupled plasma mass spectrometry (ICP−MS) by combining ultrasonic nebulization via the nitrogen mixed gas effect. We showed the effect of nitrogen gas concentration (0–5%) in the nebulizer gas on the signal sensitivity for 63 elements using commercially available (concentric and ultrasonic) nebulizers. In addition, the limit of detection (ng L^{-1}) was calculated in each case. Finally, we compared the sensitivity (i.e., the slope of the calibration curve), background noise intensity, and three-dimensional intensity distribution in the plasma to elucidate the effects of the concurrent use of mixed gas plasmas and nebulization methods.

Keywords ICP − MS · Sensitivity enhancement · Nitrogen · Mixed gas effect · Element

Introduction

The use of mixed gas plasmas in inductively coupled plasma atomic emission spectrometry (ICP−AES) and mass spectrometry (ICP−MS) is well known to offer signal enhancement [1–16]. Mixed gas plasmas minimize the mass spectral interferences resulting from the production of oxides and polyatomic ions and the matrix effect besides improving sensitivity [2, 3]. Generally, N_2 [4–12], O_2 [5, 6], and H_2 [8, 13] are prevalent additive gases, and some of them have been applied to laser ablation ICP−MS (LA−ICP−MS) [14, 15] and single-particle ICP−MS (sp ICP−MS) [16]. Although it offers an effective way to improve analytical sensitivity, it applied to the analysis of only particular elements, and not all signal intensities are enhanced. For instance, N_2 gas addition to the outer Ar gas in the ICP enhances the signal intensities of Y, Zr, and As but has no effect on Sr [5].

Fundamental studies about the mixed gas effect have been conducted via pneumatic nebulizer (i.e., concentric nebulizer; CN). Recent results obtained using ultrasonic nebulizer (USN) should be noted [12]. Signal enhancement through aerosol desolvating the aerosol produced by USN is a common technique in ICP−MS. In addition, we observed that the combination of USN and N_2 gas (2.2%) addition to the nebulizer gas enhanced the signal intensity of Sr 3.7 times compared with the use of USN alone [12]. Although Sr was used as an inert element toward the mixed gas effect in previous studies [5], our report [12] suggests that the combination of nebulization and the use of mixed gas plasma lead to a signal enhancement effect exceeding the individual impacts of the two approaches.

In this paper, we comprehensively evaluated the analytical figures of merit for 63 elements, such as the limit of detection (LOD), the slope of the calibration curve, and the background noise (BGN) intensity, when N_2 gas (0–5%) addition to the nebulizer gas was combined with CN or USN. In addition, we examined the mechanism of the mixed gas effect on USN using the three-dimensional (3D) intensity distributions in the ICP provided by shifting an ICP torch box when 1% N_2 and USN were used. Our study

✉ Yoshitaka Takagai
s015@ipc.fukushima-u.ac.jp

1 Faculty of Symbiotic Systems Science, Cluster of Science and Technology, Fukushima University, 1 Kanayagawa, Fukushima 960-1296, Japan

2 Collaborative Laboratories for Advanced Decommissioning Sciences, Sector of Fukushima Research and Development, Japan Atomic Energy Agency, 10-2, Fukasaku, Miharu, Fukushima 963-7700, Japan

3 PerkinElmer Japan Co., Ltd., 134 Godo, Hodogaya, Yokohama, Kanagawa 240-0005, Japan

4 Institute of Environmental Radioactivity, Fukushima University, 1 Kanayagawa, Fukushima 960-1296, Japan

provides new insights into the role of nebulization (CN or USN) and the mixed gas effect in enhancing the sensitivity of the elemental analysis.

Experimental

Reagents

One gram per liter (or 100 mg L^{-1}) of single-element standard solution for each of the 62 elements was used except for U. The standard solutions were purchased from FUJIFILM Wako Pure Chemical Corporation (Osaka, Japan), except Ba, Ru, Hf, Re and Ir. The solution for Ba was obtained from Kanto Chemical Co., Inc. (Tokyo, Japan), and the others were obtained from, AccuStandard, Inc. (New Haven, CT, USA). The solution for U was prepared from a multi-element mixture of 100 mg L^{-1} B, Th, and U (2% HNO_3, PerkinElmer, Inc., Waltham, MA, USA) as the single-element standard solution of U was not available in Japan. High-purity, 15.1 mol L^{-1} HNO_3 (68%, 1.4 g mL^{-1}), was purchased from Tama Chemicals Co., Ltd. (Kanagawa, Japan). The ultrapure water (with a resistivity of 18.2MΩ cm) was obtained from the PURELAB Ultra water purification system (Organo Corporation, Tokyo, Japan).

Instrumentation

A single quadrupole ICP−MS (NexION 300S, PerkinElmer) combined with a U5000AT$^+$ USN (Teledyne CETAC Technologies, Omaha, NE, USA) or quartz baffled cyclonic spray chamber with a micro-mist concentric nebulizer was used. A TruFlo sample monitor (Glass Expansion, Melbourne, Australia) was used to monitor the sample flow rate. The parameters used in the operation of ICP−MS are provided in Table S1 in Supplementary Information (SI). The 59 elements (^{7}Li, ^{9}Be, ^{11}B, ^{23}Na, ^{24} Mg, ^{27}Al, ^{45}Sc, ^{47}Ti, ^{51} V, ^{55}Mn, ^{59}Co, ^{60}Ni, ^{63}Cu, ^{66}Zn, ^{69} Ga, ^{74}Ge, ^{75}As, ^{85}Rb, ^{88}Sr, ^{89}Y, ^{90}Zr, ^{93}Nb, ^{98}Mo, ^{102}Ru, ^{103}Rh, ^{106}Pd, ^{107}Ag, ^{111}Cd, ^{115}In, ^{118}Sn, ^{121}Sb, ^{130}Te, ^{133}Cs, ^{138}Ba, ^{139}La, ^{140}Ce, ^{141}Pr, ^{142}Nd, ^{152}Sm, ^{153}Eu, ^{158}Gd, ^{159} Tb, ^{164}Dy, ^{165}Ho, ^{166}Er, ^{169}Tm, ^{180}Hf, ^{181}Ta, ^{184} W, ^{187}Re, ^{192}Os, ^{193}Ir, ^{195}Pt, ^{197}Au, ^{202}Hg, ^{205}Tl, ^{208}Pb, ^{209}Bi, and ^{238}U as monitored mass number) were measured without the use of a dynamic reaction cell (DRC) technique (i.e., STD mode). Four elements (^{39} K, ^{40}Ca, ^{52}Cr, and ^{56}Fe as monitored isotopes) were measured via the DRC mode with 1 mL min^{-1} of ammonia gas to remove interferences. A nebulizer gas flow rate not exceeding 3% of the oxide ratio to singly charged ions ($^{140}Ce^{16}O^+/^{140}Ce^+$) was obtained. It was 0.98 L min^{-1} in the only use of pure Ar and was 0.90 L min^{-1} of Ar in the case of Ar−N_2 mixed gas.

The internal diameters of quartz tubes were 17.95 mm, 13.95 mm, and 2.00 mm for the outer, middle, and injector tubes, respectively. The abbreviation "d" is the distance between the tip of the ICP torch and the sampling cone, which was 5.5 mm at the initial position. The diameter of the orifice was 1.1 mm. N_2 gas (0–50 mL min^{-1}) was mixed with 0.80–1.20 L min^{-1} of the nebulizer gas through a Y-shaped connector in the forestage of the nebulization device. 0.1 or 1 μg L^{-1} of a single-element standard solution containing 62 elements (except U), and a mixture containing U were used. The HNO_3 concentration was adjusted to 0.2 mol L^{-1}.

Evaluation and calculations

The effect of two different types of nebulization (CN or USN) on the Ar−N_2 mixed plasma was examined using three evaluation criteria, sensitivity enhancement ratio (SER), BGN, and LOD. The concentrations of 0.1 and 1 μg L^{-1} standard solutions (dissolved in 0.2 mol L^{-1} HNO_3) and blank solutions (0.2 mol L^{-1} HNO_3 solution) were measured via CN and USN, respectively; then, their sensitivities (i.e., cps/(μg L^{-1})) were calculated the net intensity after the subtraction of the BGN (cps) was divided by the concentration (μg L^{-1}) of the standard solution. To avoid spectral interference, single-element standard solutions were used in this study, while U was used as a mixed solution due to legal regulation. In the acquisition of signal intensity, the average intensity was calculated from 25 measurements. The SERs were calculated as the ratio of the sensitivity in the presence or absence of N_2 by the following equation:

$$SER = \frac{Sensitivity_{Ar-N_2}}{Sensitivity_{Ar}} \quad (1)$$

where $Sensitivity_{Ar}$ (cps/(μg L^{-1})) and $Sensitivity_{Ar-N_2}$ (cps/(μg L^{-1})) represent the sensitivity of a pure Ar plasma and that in the presence of N_2 in Ar gas, respectively.

The 3-sigma method based on the Gaussian distribution model is commonly used for the calculation of LODs; in the case of very low signal intensities, the Poisson distribution is suitable to determine the LOD [17]. In this study, LOD values were calculated using the upper limit (L_c) of the 95% one-sided confidence interval based on the Poisson distribution model [17].

$$LOD = 2L_c \times Sensitivity \quad (2)$$

where Sensitivity (cps/(μg L^{-1})) represents the slope of the calibration curve. The BGN of the 95% confidence interval was calculated using free software R [18].

3D intensity distribution in the plasma

The 3D intensity distribution of target ions in the plasma was obtained by changing the distance between the ICP torch and the sampling cone. ^{9}Be, ^{88}Sr, and ^{208}Pb were selected as the

typical two model cases in the activated elements (^{9}Be and ^{88}Sr) and the inert elements (^{208}Pb), and 0.1 µg L^{-1} of the single-element standard solution (Be, Sr, and Pb) in 0.2 mol L^{-1} HNO_3 was measured via USN. The nebulizer gas flow rate was 1.04 L min^{-1} in the absence of N_2. In contrast, the nebulizer gas flow rate was 1.03 L min^{-1} in the presence of 1% N_2 (10 mL min^{-1}). An interval distance (*Z*-axis) between the torch and the sampling cone (i.e., sampling depth) and an alignment (*X*- and *Y*-axis) were controlled by software for ICP−MS. The sampling depth was defined as an initial point at 5.5 mm, and distance variation was adjusted at 1.5 mm intervals in the region from 2.5 mm to 8.5 mm. The lateral signal intensity was measured in 0.6 mm increments between − 2.4 mm and + 2.4 mm to the position of the orifice.

In addition, the transition of intensity distribution by adding N_2 into the nebulizer gas was investigated. 0.1 µg L^{-1} of the single-element standard solution (Be, Sr, Ce, and Pb) in 0.2 mol L^{-1} HNO_3 was measured. The transition degree (T%) was calculated by the following equation:

$$T\% = \left(\frac{I_{x(Ar-N_2)}}{I_{max(Ar-N_2)}} - \frac{I_{x(Ar)}}{I_{\max(Ar)}} \right) \times 100 \quad (3)$$

where $I_{x(Ar\text{-}N_2)}$ and $I_{max(Ar\text{-}N_2)}$ represent the signal intensity at the point and the maximum intensity at the depth in the presence of 1% N_2, respectively. $I_{x(Ar)}$ and $I_{max(Ar)}$ represent the signal intensity at the point and the maximum intensity at the depth in the absence of N_2, respectively.

Results and discussion

Effect of nebulization (CN or USN) on SER in Ar − N_2 mixed plasma

Table 1 shows the sensitivity (in pure Ar plasma and Ar−N_2 mixed plasma) and SER values of the 63 elements measured via CN or USN. In 53 elements, the sensitivity was improved by the Ar−N_2 mixture via CN (SER > 1). In contrast, the sensitivity for 35 elements was improved by the Ar−N_2 mixture via USN. The results are summarized in (Fig. 1), and each circle means the respective elements. The circle size and the color represent the mass number of each element. The error bars show the propagation error of SER calculated from the standard deviation of signal intensity in absence of N_2 and presence of 1% N_2. The circles above the equivalent line (y = x) show higher SER via USN than CN, and below show higher SER via CN than USN. The circles on the line indicate that there is no difference in SER measured via USN and CN.

Among 18 of the improved 35 elements in USN (SER > 1), the values are higher than those in CN (^{7}Li, ^{9}Be, ^{11}B, ^{23}Na, ^{47}Ti, ^{51} V, ^{55}Mn, ^{59}Co, ^{60}Ni, ^{63}Cu, ^{66}Zn, ^{69} Ga, ^{74}Ge, ^{75}As, ^{85}Rb, ^{88}Sr, ^{89}Y, and ^{103}Rh). The gray-colored area having both SER values less than 1 for CN and USN represents the inert zone toward the addition effect of N_2 into Ar plasma (8 elements: ^{56}Fe, ^{111}Cd, ^{130}Te, ^{192}Os, ^{193}Ir, ^{195}Pt, ^{197}Au, and ^{202}Hg). ^{106}Pd had a SER > 1; nevertheless, the values were nearly 1. Many of them were platinum group elements, Cd and Hg. The solid linear line (y = x ± 5%) means that the equivalent SER values are obtained in the case of CN and USN. In other words, the elements on this line are those that do not dominance between CN and USN in the sensitivity enhancement obtained by the Ar−N_2 effect (6 elements: ^{45}Sc, ^{90}Zr, ^{93}Nb, ^{102}Ru, ^{107}Ag, and ^{118}Sn). In addition, the circle size and its color indicate an intense tendency that use of USN is effective for elements lower than *m/z* 100 except ^{103}Rh.

Figure 2 shows the impact of the concentration of N_2 gas (0–5%) on the ratio of the resultant intensity (with N_2) to original intensity (without N_2). The ratio was calculated from each of the intensities obtained via CN and USN. The value 1 was defined as the same intensity as that without N_2. N_2 flow rate within 1% of nebulizer gas flow rate was optimum for most elements. The dependency of additive gas flow rate on sensitivity enhancement effect seems to have occurred because of shifting ionization region in the ICP, therefore, we investigated about this inference by plotting a 3D intensity distribution in the next chapter.

3D relative intensity distribution in the ICP

The signal intensity distribution measured by changing the positional relationship of the ICP torch to the orifice represents the actual distribution of target ions in the ICP [19]. Namely, the place showing the maximum signal intensity means that the target analyte is the most ionized at the position. The 3D distribution of the relative intensity based on the background intensity is shown in (Fig. 3). It was observed by changing the ICP position axially and laterally to the orifice. 0.1 µg L^{-1} single-element standard solution of three elements (^{9}Ba, ^{88}Sr, and ^{208}Pb) were measured via CN in (a) the absence of N_2 and (b) the presence of 1% N_2; furthermore, they were also measured via USN in (c) the absence of N_2 and (d) the presence of 1% N_2. ^{9}Be and ^{88}Sr had SERs activated by N_2 in USN. In contrast, ^{208}Pb was selected as a SER-inert element in N_2 addition via USN. Moreover, the elements (typically, ^{9}Be and ^{88}Sr) with *m/z* lower than 100 showed little response to the addition of N_2 at any distance via CN, the element above *m/z* 100 (typically ^{208}Pb) was slightly activated at the distance via CN. Relatively, the elements with *m/z* lower than 100 were significantly activated via USN; in contrast, Pb was not activated via USN. While the distance between the torch and the sampling cone increased, the high intensity was even

Table 1 The comparison of the sensitivity enhancement ratio (SER)

Element	*m/z*	Sensitivity (cps / μg L^{-1})				SER	
		CN		USN		CN	USN
		Ar	$Ar-N_2$	Ar	$Ar-N_2$	$(Ar-N_2/Ar)$	$(Ar-N_2/Ar)$
Li	7	34,175	51,091	129,524	220,196	1.49 ± 0.11	1.70 ± 0.07
Be	9	9590	13,701	14,780	29,722	1.43 ± 0.10	2.01 ± 0.06
B	11	12,641	6471	9714	13,535	0.51 ± 0.02	1.39 ± 0.20
Na	23	91,394	103,646	139,697	217,249	1.13 ± 0.03	1.56 ± 0.04
Mg	24	43,527	75,741	138,570	185,734	1.74 ± 0.13	1.34 ± 0.03
Al	27	68,248	111,768	108,498	138,003	1.64 ± 0.12	1.27 ± 0.10
K	39	2102	4951	15,132	10,353	2.36 ± 5.59	0.65 ± 0.05
Ca	40	20,403	74,649	198,065	74,559	3.66 ± 3.35	0.38 ± 0.05
Sc	45	52,943	113,660	82,973	179,519	2.15 ± 0.19	2.16 ± 0.31
Ti	47	3903	4018	13,423	31,490	1.03 ± 0.26	2.35 ± 0.04
V	51	43,818	102,381	100,078	263,170	2.34 ± 0.18	2.63 ± 0.11
Cr	52	66,099	89,739	38,976	32,120	1.36 ± 0.45	0.80 ± 0.06
Mn	55	71,345	146,482	97,674	270,010	2.05 ± 0.05	2.76 ± 0.08
Fe	56	40,798	34,092	81,137	63,172	0.84 ± 0.06	0.78 ± 0.06
Co	59	37,055	80,243	79,889	202,524	2.17 ± 0.16	2.54 ± 0.05
Ni	60	10,447	18,406	16,738	41,757	1.76 ± 0.19	2.49 ± 0.09
Cu	63	29,285	37,449	43,791	116,956	1.28 ± 0.03	2.67 ± 0.08
Zn	66	3830	3905	8481	14,290	1.02 ± 0.01	1.68 ± 0.03
Ga	69	26,703	62,934	50,578	147,334	2.36 ± 0.17	2.91 ± 0.06
Ge	74	9479	13,246	12,976	21,939	1.40 ± 0.02	1.69 ± 0.08
As	75	3794	3729	13,533	27,552	0.98 ± 0.02	2.04 ± 0.15
Rb	85	41,476	56,322	61,532	140,559	1.36 ± 0.02	2.28 ± 0.08
Sr	88	75,060	141,696	295,820	677,856	1.89 ± 0.17	2.29 ± 0.16
Y	89	58,078	88,285	215,306	426,695	1.52 ± 0.03	1.98 ± 0.12
Zr	90	22,873	36,813	58,626	92,482	1.61 ± 0.03	1.58 ± 0.05
Nb	93	44,300	74,231	81,898	143,389	1.68 ± 0.02	1.75 ± 0.09
Mo	98	11,120	19,507	20,501	32,885	1.75 ± 0.02	1.60 ± 0.02
Ru	102	16,556	24,017	30,973	44,560	1.45 ± 0.04	1.44 ± 0.03
Rh	103	49,537	66,494	82,486	153,110	1.34 ± 0.03	1.86 ± 0.05
Pd	106	12,295	14,924	12,660	14,470	1.21 ± 0.03	1.14 ± 0.05
Ag	107	23,880	25,261	54,392	56,600	1.06 ± 0.02	1.04 ± 0.03
Cd	111	6091	4940	18,471	8401	0.81 ± 0.02	0.45 ± 0.01
In	115	97,558	137,012	67,588	79,962	1.40 ± 0.10	1.18 ± 0.08
Sn	118	14,431	15,087	96,756	100,971	1.05 ± 0.05	1.04 ± 0.03
Sb	121	12,529	12,779	62,299	42,747	1.02 ± 0.04	0.69 ± 0.01
Te	130	3771	2680	21,517	8749	0.71 ± 0.04	0.41 ± 0.01
Cs	133	83,855	111,063	173,851	150,700	1.32 ± 0.09	0.87 ± 0.02
Ba	138	64,695	86,666	160,326	161,191	1.34 ± 0.10	1.01 ± 0.04
La	139	115,611	178,178	205,096	217,727	1.54 ± 0.09	1.06 ± 0.03
Ce	140	74,179	104,248	120,572	120,034	1.41 ± 0.10	1.00 ± 0.11
Pr	141	50,959	66,088	194,966	181,591	1.30 ± 0.11	0.93 ± 0.06
Nd	142	10,384	14,918	51,472	47,459	1.44 ± 0.26	0.92 ± 0.07
Sm	152	11,181	20,212	32,938	32,654	1.81 ± 0.28	0.99 ± 0.15
Eu	153	18,395	31,409	94,819	94,183	1.71 ± 0.26	0.99 ± 0.06
Gd	158	10,665	20,082	36,066	35,325	1.88 ± 0.40	0.98 ± 0.04
Tb	159	40,448	70,509	124,417	128,557	1.74 ± 0.28	1.03 ± 0.13
Dy	164	11,821	20,631	88,859	59,421	1.75 ± 0.26	0.67 ± 0.03
Ho	165	34,514	65,193	178,476	179,134	1.89 ± 0.27	1.00 ± 0.09

Table 1 (continued)

Element	*m/z*	Sensitivity (cps / μg L^{-1})				SER	
		CN		USN		CN	USN
		Ar	Ar – N_2	Ar	Ar – N_2	(Ar – N_2/Ar)	(Ar – N_2/Ar)
Er	166	9688	20,121	47,497	44,173	2.08 ± 0.26	0.93 ± 0.10
Tm	169	52,268	95,985	153,864	124,320	1.84 ± 0.26	0.81 ± 0.04
Hf	180	9137	12,296	61,565	54,020	1.35 ± 0.03	0.88 ± 0.02
Ta	181	92,582	129,696	232,761	182,189	1.40 ± 0.13	0.78 ± 0.02
W	184	25,232	34,489	46,356	31,889	1.37 ± 0.11	0.69 ± 0.02
Re	187	23,218	31,473	97,468	70,540	1.36 ± 0.04	0.72 ± 0.01
Os	192	18,039	16,506	113,284	69,313	0.92 ± 0.02	0.61 ± 0.03
Ir	193	50,191	39,020	170,684	87,476	0.78 ± 0.02	0.51 ± 0.02
Pt	195	6934	4087	35,838	12,350	0.59 ± 0.01	0.34 ± 0.01
Au	197	8898	4878	45,943	17,001	0.55 ± 0.01	0.37 ± 0.01
Hg	202	13,585	6684	59,184	28,491	0.49 ± 0.04	0.48 ± 0.01
Tl	205	66,096	82,816	141,738	159,249	1.25 ± 0.09	1.12 ± 0.13
Pb	208	44,933	59,326	68,985	49,812	1.32 ± 0.09	0.72 ± 0.02
Bi	209	71,268	87,157	74,833	49,810	1.22 ± 0.09	0.67 ± 0.20
U	238	93,230	112,532	421,135	457,647	1.21 ± 0.09	1.09 ± 0.02

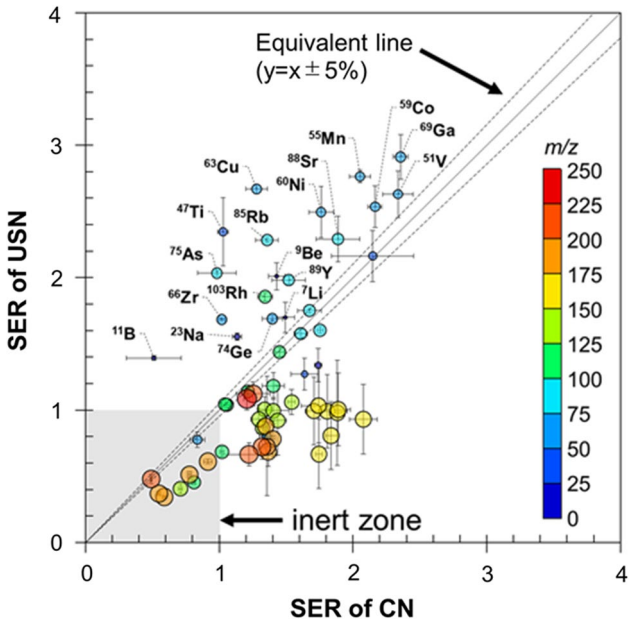

Fig. 1 Relationship between sensitivity enhancement ratios (SERs) of USN and CN. The size and color of circles indicate *m/z*

maintained in the case of USN. These 3D distributions indicate that N_2 addition assisted the extension and stabilization of the ionized regions. Mixtures of Ar and N_2 have a high thermal conductivity at temperatures between 5000 and 10,000 K [20]; therefore, the Ar–N_2 mixture contributes to LOD improvement via signal enhancement.

Figure 4 shows the transition (T%) of the signal intensity via USN from the absence of N_2 to the presence of N_2 for four elements (^{9}Be, ^{88}Sr, ^{140}Ce, and ^{208}Pb). The red color shows that the signal intensity at a given point increased in the presence of 1% N_2 compared to that in the absence of N_2. The blue color shows that the signal intensity at a given point decreased in the presence of 1% N_2 compared to that in the absence of N_2. For the elements with *m/z* lower than 100, such as ^{9}Be and ^{88}Sr, the maximum intensities were expanded from the torch side (short distance of "d") to the sampling cone side (long distance of "d"). In contrast, the positions of maximum intensities were shifted to the plasma side for the element with *m/z* larger than 100, such as ^{140}Ce and ^{208}Pb. Since an ordinary distance of "d" is 5.5 mm for detection, it seems difficult to find the optimum point of the maximum intensity resulting from the shift, which is caused by N_2 addition, in the measurement of elements with *m/z* above 100. N_2 effects via USN for elements with *m/z* above 100 might require special configurations for the position adjustment between the torch and sampling cone.

Impact of Ar–N_2 mixed plasma on background noise intensity (BGN)

Table S2 in SI shows the impact of Ar–N_2 mixed plasma on BGN (in the measurement of 0.2 mol L^{-1} HNO_3 as a blank solution), and the interference ions reported in the literature [21–24] were also listed. In the presence of N_2 in Ar plasma, both detrimental (i.e., increase of BGN) and beneficial (i.e., decrease of BGN) effects were confirmed. The detrimental effect is occurred due to the generation of polyatomic ions (containing N atoms) based on the charge transfer reaction between N_2 and Ar [25]. For instance, the intensity of *m/z* 55 (position for ^{55}Mn) was significantly increased by the generation of $^{40}Ar^{15}N^{+}$ and $^{40}Ar^{14}N^{1}H^{+}$. The detrimental

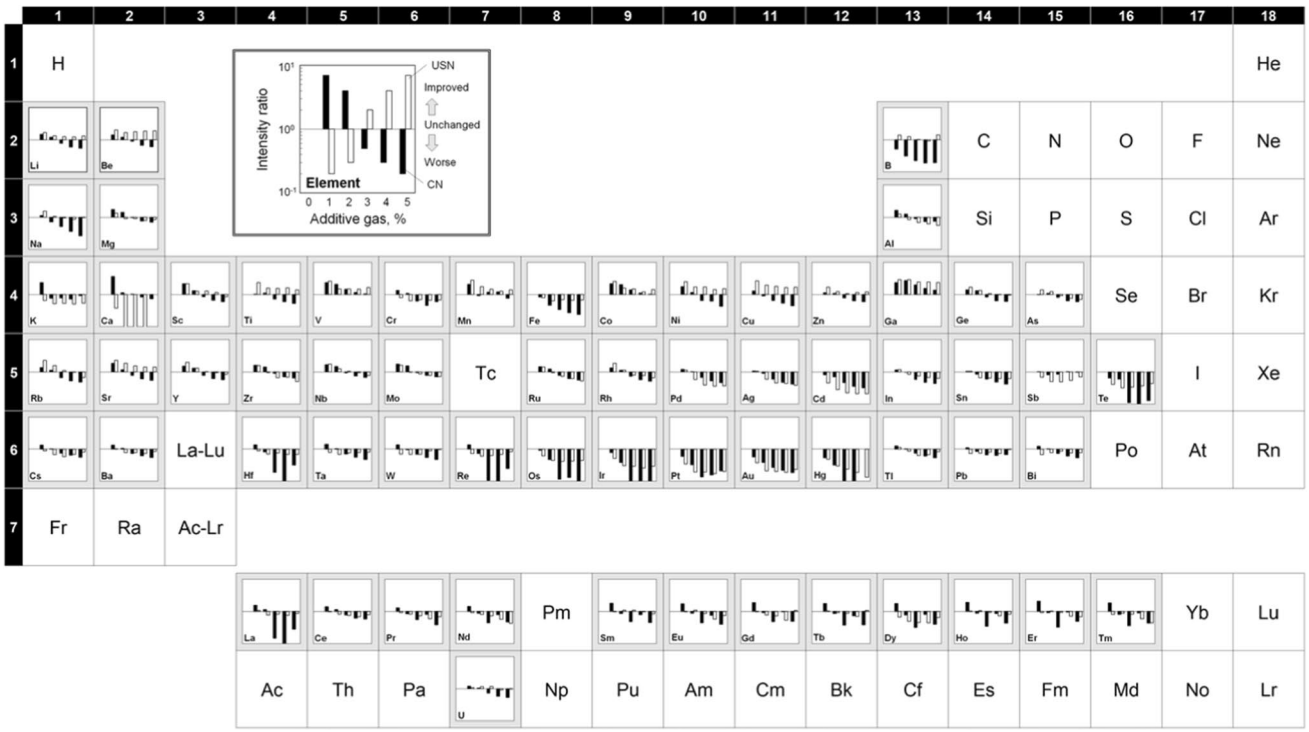

Fig. 2 Impact of the concentration of N_2 gas on the ratio of resultant intensity (with N_2) to original intensity (without N_2). Nebulizer gas flow rate not exceeding 3% of CeO/Ce was optimized. The intensities were obtained via concentric (CN, black bar) and ultrasonic nebulizers (USN, white bar). Sample: 0.1 μg L^{-1} in 0.2 mo L^{-1} HNO_3

effects such as spectral interferences were observed on *m/z* 27, 45, 47, 51, 52, and 56 (position for ^{27}Al, ^{45}Sc, ^{47}Ti, ^{51} V, ^{52}Cr, and ^{56}Fe, respectively). In contrast, the beneficial effect can be seen in the intensities of *m/z* 39, 40, and 66 (position for ^{39} K, ^{40}Ca, and ^{66}Zn, respectively) as the decrease of BGN. Typically, the interference ions toward ^{39} K, ^{40}Ca, and ^{66}Zn appear on those *m/z* positions in pure Ar plasma due to the generation of polyatomic ions containing Ar or O atoms. Specific examples of interfering ion are below: $^{38}ArH^+$ on $^{39}K^+$, $^{40}Ar^+$ on $^{40}Ca^+$, and $^{34}S^{16}O_2^+$ on $^{66}Zn^+$ as shown in Table 2S. The Ar volume is relatively reduced by the N_2 volume increase in the plasma; thus, the resultant the generation of Ar-derived interference ions decreased.

Moreover, Fig. 5A shows the BGN suppression efficiency in the case of CN or USN in the absence or presence of N_2. Each circle means respective elements. In both USN and CN, the BGN in the presence of N_2 was lower than that in the absence of N_2 indicating that N_2 addition suppresses BGN for both CN and USN. Figure 5B shows the relationship between *m/z* and the mean square of the improvement degree in BGN ($\sqrt{\chi^2}$). χ represents the root-square value that the difference value of BGNs obtained via CN and USN in Ar−N_2 is divided by BGN of CN in Ar−N_2. From the results, the suppression effect of USN (via Ar−N_2) works for *m/z* lower than 120; however, it became relatively worse on higher *m/z* values. Although the suppression effect (by N_2 addition) does not discriminate between CN and USN based on the result of (Fig. 5A), it contributes mainly to *m/z* less than 120.

Limit of detection

Table 2 shows the LODs calculated from the upper limit of the 95% one-sided confidence interval of the observed background intensity and sensitivity. The LODs were improved 3.3-fold (median) by combination between Ar−N_2 and USN as compared with the general method (i.e., the combination of pure Ar and CN). While LOD did not improve regarding 9 elements (Al, Mn, Ga, Ge, Te, Ce, Tm, Os, and Bi), the present method (i.e., the combination of Ar−N_2 and USN) is of benefit to other elements. Figure 6 exhibits the LOD improvement factors on each *m/z*. The values were calculated by the ratio of the LODs in USN and CN via the presence or absence of N_2. The LOD improvement depended on the character of the element. For some elements, the LOD was lower in the presence of N_2, while for others, the LOD was lower in the absence of N_2. Regardless of the nebulization method used, the effect of N_2 addition was ineffective for the *m/z* range of 139–169 (lanthanides). The *m/z* 7(Li), 9(Be), 47(Ti), 75 to 89(As to Y), 102(Ru), and 103(Rh) showed a tendency for decreased LOD by the addition of N_2 in USN. This is attributed to the effect of N_2 in USN

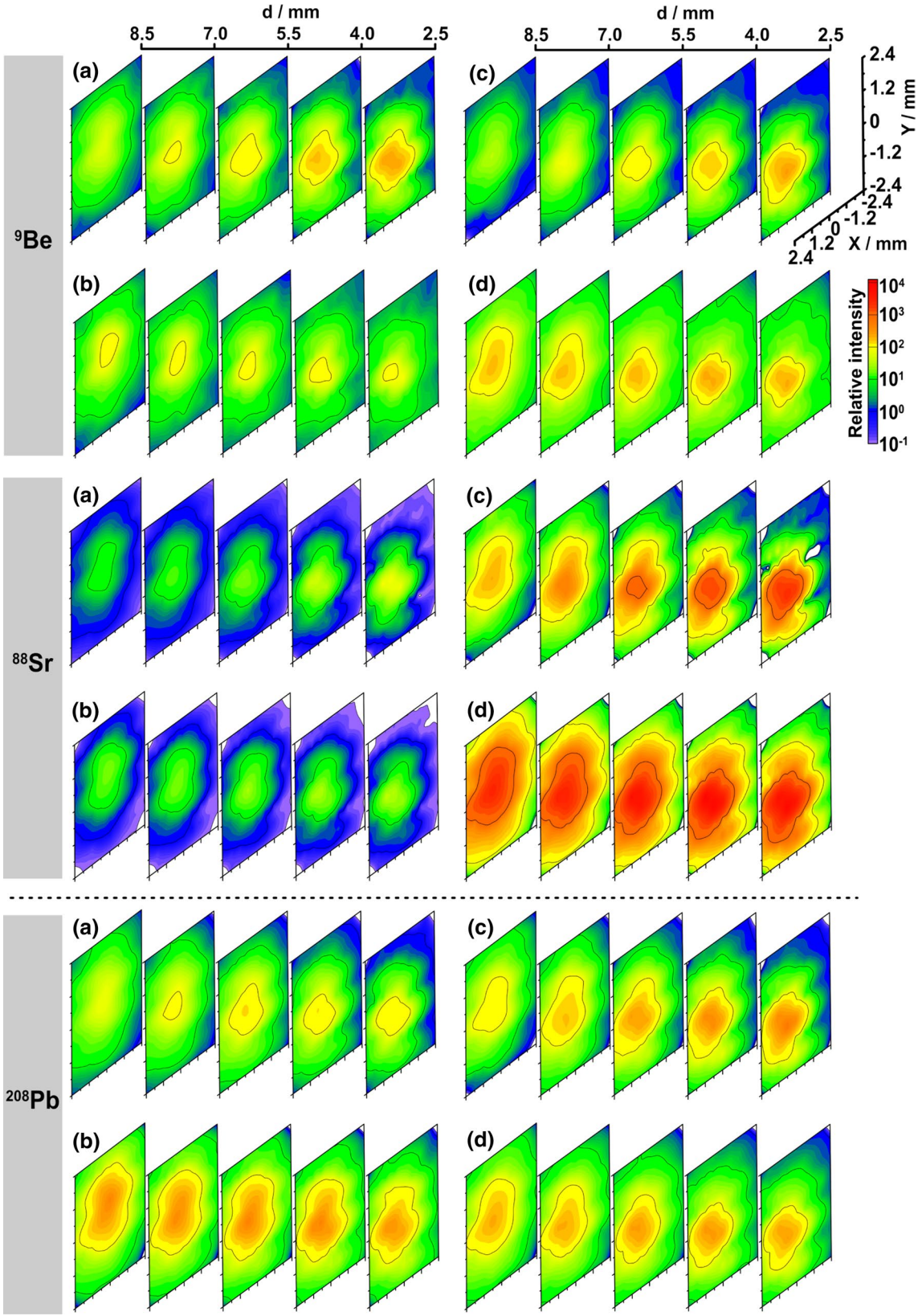

Fig. 3 3D distribution of the relative ratio of the intensity to the background intensity in the **a** absence of N_2 via CN or **b** presence of 1% N_2 via CN; **c** absence of N_2 via USN or **d** presence of 1% N_2 via USN. Each intensity was measured at different sampling depths (2.5–8.5 mm)

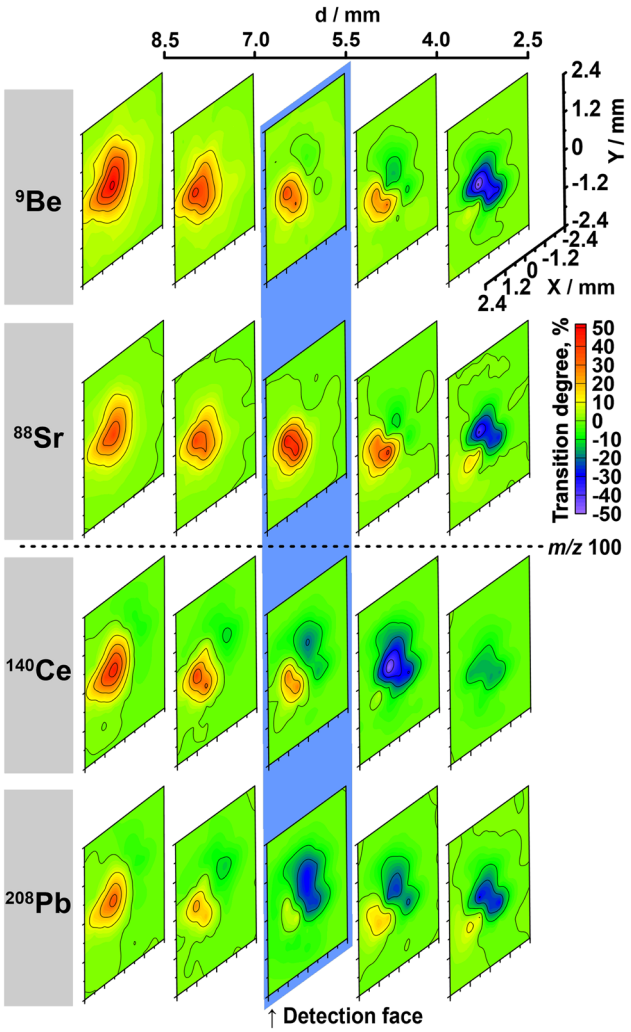

Fig. 4 Transition (T%) of the position of the maximum intensity by adding N_2 via USN. The standard detection face was the 5.5 mm distance between the plasma and the torch

(i.e., increase in SER) and the low SD of the BGN. For the elements with *m/z* above 180, the SER improvement by N_2 was observed in CN; thus, it would greatly improve the LOD of CN.

Conclusion

The improvement in analytical performance by combining Ar−N_2 gas addition into the nebulizer with different nebulization methods (i.e., CN and USN) in ICP−MS for 63 elements was reported. We showed the effect of the N_2 gas concentration range 0–5% in the nebulizer gas on the analytical performance for 63 elements via commercially available nebulization methods (CN and USN). The SERs, BGNs, and LODs were investigated. Our results showed there was a tendency of SER improvement for elements lower than *m/z* than 100 using USN and mixed gas effect. In addition, 3D intensity distributions in the plasma were discussed to characterize the mixed gas effect and the mechanism of the sensitivity improvement. The 3D distributions indicated that N_2 addition assisted the extension and stabilization of the ionized regions due to their high thermal conductivity. In addition, the transition of the maximum intensity to the torch side was found, especially for elements lower than *m/z* 100. The use of USN as a desolvation tool helped in decreasing the BGN. Mixed Ar−N_2 plasma caused the generation of N-derived polyatomic ions such as $^{40}Ar^{15}N^+$. On the other hands, the generation of Ar-derived interference ions decreased. LOD was calculated in each case. From those results, the improvement in analytical performance using USN and Ar−N_2 as with CN and Ar−N_2 is considered. The insights obtained in this study are as follows:

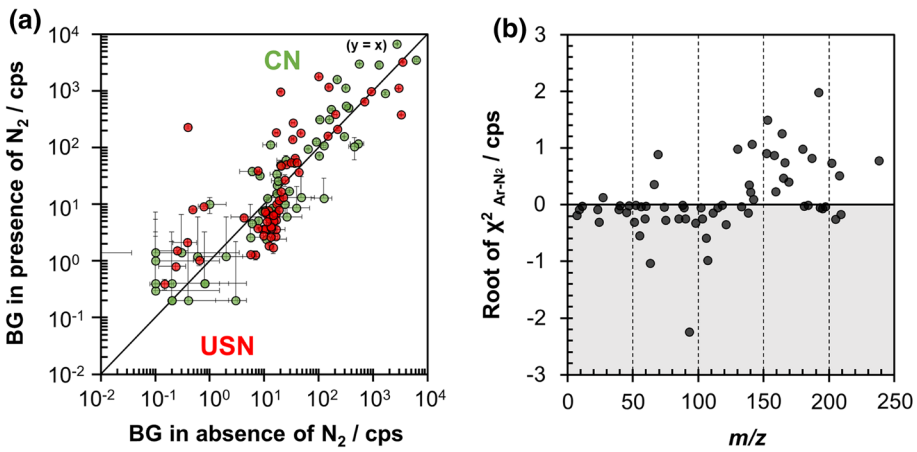

Fig. 5 The relationship of BGN in between absence of N_2 and presence of 1% N_2 via USN (red circle) and CN (green circle) (**A**) and the *m/z* dependence on BGN (**B**). The error bars in **A** show the standard deviation of BGN

Table 2 The obtained LOD with or without N_2 via CN or USN

Element	*m/z*	LOD / ng L^{-1}			
		CN		USN	
		Ar	Ar−N_2	Ar	Ar−N_2
Li	7	12	20	2.7	1.7
Be	9	2.7	7.7	3.5	1.0
B	11	279	300	241	275
Na	23	244	377	52	31
Mg	24	5.1	4.0	0.74	0.89
Al	27	12	9.8	3.3	18
K	39	6087	1475	95	134
Ca	40	2021	338	35	11
Sc	45	108	122	3.0	21
Ti	47	128	832	5.5	4.3
V	51	16	12	0.95	2.3
Cr	52	559	902	50	65
Mn	55	41	1645	14	639
Fe	56	66	175	6.3	7.7
Co	59	8.0	3.3	0.77	0.62
Ni	60	116	339	3.3	10
Cu	63	2.5	4.1	2.0	1.2
Zn	66	300	72	55	60
Ga	69	1.7a	4.3	1.2	14
Ge	74	17	17	9.6	19
As	75	14	17	4.0	1.3
Rb	85	1.3	0.88	0.88	0.22
Sr	88	4.0	5.0	0.20	0.047
Y	89	1.4	0.62	0.19	0.034
Zr	90	1.5	0.86	1.0	0.45
Nb	93	0.83	0.42	0.51	0.22
Mo	98	3.8	2.3	1.9	0.94
Ru	102	1.9	3.8	1.1	0.46
Rh	103	0.95	0.51	0.48	0.13
Pd	106	2.6	1.6	2.5	1.4
Ag	107	2.6	5.2	2.0	2.5
Cd	111	4.3	4.7	1.7	1.3
In	115	1.0	1.0	0.62	0.33
Sn	118	49	160	0.71	0.44
Sb	121	3.1	1.6	0.87	0.55
Te	130	263	95	284	271
Cs	133	0.65	0.86	0.21	0.12
Ba	138	0.88	0.88	0.23	0.19
La	139	0.10	0.041	0.13	0.051
Ce	140	0.15	0.35	0.59	0.65
Pr	141	0.22	0.11	0.25	0.13
Nd	142	1.1	0.75	1.0	0.37
Sm	152	0.66	0.37	1.7	0.63
Eu	153	0.40	0.23	0.52	0.28
Gd	158	0.69	0.37	1.4	0.41
Tb	159	0.18	0.16	0.38	0.16
Dy	164	0.62	0.36	0.23	0.44
Ho	165	0.21	0.17	0.25	0.11
Er	166	0.76	0.37	0.94	0.40
Tm	169	0.14	0.12	0.26	0.19
Hf	180	0.81	0.60	0.12	0.27
Ta	181	7.1	2.8	0.032	0.17
W	184	9.8	5.3	0.16	0.35
Re	187	0.62	0.35	0.11	0.48
Os	192	2.2	0.88	0.065	7.6
Ir	193	2.5	1.1	0.043	0.17
Pt	195	3.8	4.3	0.21	0.60
Au	197	33	9.1	0.24	0.66
Hg	202	5.6	3.9	0.53	3.7
Tl	205	3.8	8.5	0.65	2.1
Pb	208	2.4	0.58	1.7	2.0
Bi	209	1.0	0.42	0.83	1.1
U	238	0.19	0.066	0.018	0.024

- The use of USN was more effective for light elements ($m/z < 100$ excluding ^{103}Rh). In contrast, the use of CN was more effective for heavy elements on signal enhancement effect with use of Ar−N_2 (1% N_2). However, most elements in the platinum group were inert.
- The mass number dependence of the signal enhancement effect has explained by shifting the ionization region obtained from ion intensity distribution in the ICP.
- The effect of background reduction (especially, for light elements having $m/z < 120$) caused by reduction of solvent-derived polyatomic ion interference was observed when Ar−N_2 was combined with USN.
- LOD was improved as a result of signal enhancement and background reduction effect, therefore, USN was advantageous for light elements and CN was advantageous for heavy elements in many cases.

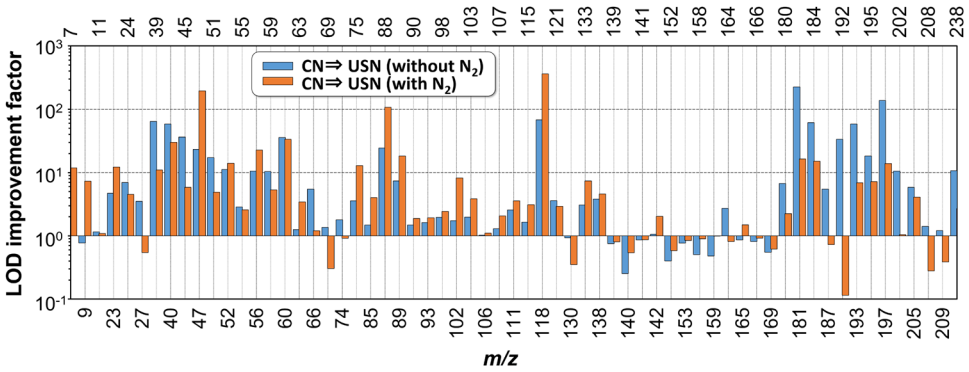

Fig. 6 The LOD improvement factor. The blue and orange bars show the ratio of LODs between USN and CN via the absence or presence of 1% N_2, respectively

Supplementary Information The online version contains supplementary material available at https://doi.org/10.1007/s44211-022-00140-4.

Acknowledgements The authors gratefully acknowledge funding by the JAEA Nuclear Energy S&T and Human Resource Development Project through concentrating wisdom Grant Number JPJA19H19210081, and the Japan Society for the Promotion of Science (JSPS) Grant-in-Aid for Scientific Research (B) 20H04352.

References

1. G.L. Scheffler, D. Pozebon, Anal. Methods **6**, 6170 (2014)
2. C. Agatemor, D. Beauchemin, Spectrochim. Acta, Part B **66**, 1 (2011)
3. G.L. Scheffler, D. Pozebon, D. Beauchemin, J. Anal. At. Spectrom. **33**, 1269 (2018)
4. E.H. Choot, G. Horlick, Spectrochim. Acta, Part B **41**, 889 (1986)
5. J.W.H. Lam, G. Horlick, Spectrochim. Acta, Part B **45**, 1313 (1990)
6. E.H. Evans, L. Ebdon, J. Anal. At. Spectrom. **5**, 425 (1990)
7. D. Beauchemin, J.M. Craig, Spectrochim. Acta, Part B **46**, 603 (1991)
8. H. Louie, S.Y. Soo, J. Anal. At. Spectrom. **7**, 557 (1992)
9. K. Wagatsuma, K. Hirokawa, Anal. Sci. **9**, 509 (1993)
10. M. Ohata, Anal. Sci. **32**, 219 (2016)
11. Y. Makonnen, W.R. MacFarlane, M.L. Geagea, D. Beauchemin, J. Anal. At. Spectrom. **32**, 1688 (2017)
12. M. Furukawa, M. Matsueda, Y. Takagai, Anal. Sci. **34**, 471 (2018)
13. L. Ebdon, M.J. Ford, P. Goodall, S.J. Hill, Microchem. J. **48**, 246 (1993)
14. T. Hirata, R.W. Nesbitt, Geochim. Cosmochim. Acta **59**, 2491 (1995)
15. Z. Hu, S. Gao, Y. Liu, S. Hu, H. Chen, H. Yuan, J. Anal. At. Spectrom. **23**, 1093 (2008)
16. J. Kofsky, D. Beauchemin, Spectroscopy **35**, 22 (2020)
17. M. Tanner, J. Anal. At. Spectrom. **25**, 405 (2010)
18. R Core Team, R: A language and environment for statistical computing, R Foundation for Statistical Computing (Vienna, Austria, 2021), https://www.R-project.org/. Accessed 31 Mar 2022
19. J.H. Macedone, A.A. Mills, P.B. Farnsworth, Appl. Spectrosc. **58**, 463 (2004)
20. A.B. Murphy, C.J. Arundelli, Plasma Chem. Plasma Process. **14**, 451 (1994)
21. T.W. May, R.H. Wiedmeyer, At. Spectrosc. **19**, 150 (1998)
22. S. D'llio, N. Violante, C. Majorani, F. Petrucci, Analytica. Chimica. Acta. **698**, 6 (2011)
23. J.E. O'Sullivan, R.J. Watson, E.C.V. Butler, Talanta **115**, 999 (2013)
24. C. Neff, P. Becker, B. Hattendorf, D. Günther, J. Anal. At. Spectrom. **36**, 1750 (2021)
25. R.S. Houk, A. Montaster, V.A. Fassel, Appl. Spectrosc. **37**, 425 (1983)